# Pharmacologically inducing regenerative cardiac cells by small molecule drugs

Wei Zhou[1,2,†], Kezhang He[2,†], Chiyin Wang[3], Pengqi Wang[2], Dan Wang[2], Bowen Wang[1,2], Han Geng[2], Hong Lian[3], Tianhua Ma[2]*, Yu Nie[3]*, Sheng Ding[1,2,4]*

**Affiliations**

[1]Tsinghua-Peking Joint Center for Life Sciences, Tsinghua University, Beijing 100084, China

[2]School of Pharmaceutical Sciences, Tsinghua University, Beijing 100084, China

[3]State Key Laboratory of Cardiovascular Disease, Fuwai Hospital, National Center for Cardiovascular Disease, Chinese Academy of Medical Sciences and Peking Union Medical College, Beijing, 100037, China

[†]W.Z. and K.Z.H. contributed equally to this work.

[4]Lead contact

*Corresponding author. Email: matianhua@tsinghua.edu.cn (T.M.), nieyu@fuwaihospital.org (Y.N.), shengding@tsinghua.edu.cn (S.D.)

**Summary**

Adult mammals, unlike some lower organisms, lack the ability to regenerate damaged hearts through cardiomyocytes (CMs) dedifferentiation into cells with regenerative capacity. Developing conditions to induce such naturally unavailable cells with potential to proliferate and differentiate into CMs, i.e., regenerative cardiac cells (RCCs), in mammals will provide new insights and tools for heart regeneration research. In this study, we demonstrate that a two-compound combination, CHIR99021 and A-485 (2C), effectively induces RCCs from human embryonic stem cell (hESC)-derived TNNT2$^{+}$ CMs *in vitro*, as evidenced by lineage tracing experiments. Functional analysis shows that these RCCs express a broad spectrum of cardiogenesis genes and have the potential to differentiate into functional CMs, endothelial cells (ECs), and smooth muscle cells (SMCs). Importantly, similar results were observed in neonatal rat CMs both *in vitro* and *in vivo*. Remarkably, administering 2C in adult mouse hearts significantly enhances survival and improves heart function post-myocardial infarction. Mechanistically, CHIR99021 is crucial for the transcriptional and epigenetic activation of genes essential for RCC development, while A-485 primarily suppresses H3K27Ac and particularly H3K9Ac in CMs. Their synergistic effect enhances these modifications on RCC genes, facilitating the transition from CMs to RCCs. Therefore, our findings demonstrate the feasibility and reveal the mechanisms of pharmacological induction of RCCs from endogenous CMs, which could offer a promising regenerative strategy to repair injured hearts.

## Main Text

Lower organisms like zebrafish exhibit a remarkable capacity for cardiac regeneration through CM dedifferentiation, characterized by the reactivation of embryonic cardiogenic genes and disassembly of sarcomeric structures (Kikuchi & Poss, 2010; Lepilina et al., 2006). In contrast, mammals show limited cardiac regeneration, typically restricted to the early postnatal period (PN1 to PN6) in mice, beyond which the regenerative ability sharply declines (Porrello et al., 2011). This stark difference underscores the need for novel strategies to induce a regenerative state in adult mammalian CMs, akin to that observed in zebrafish, to overcome the inherent barriers to CM dedifferentiation.

During mammalian heart development, CMs arise predominantly from the first heart field (FHF) and the second heart field (SHF) (Srivastava, 2006), with SHF cells marked by the pioneer transcription factor ISL1 proliferating and differentiating into major cardiovascular cell types, CMs, SMCs and ECs during embryonic development (Bu et al., 2009; Moretti et al., 2006). Notably, ISL1$^+$ cells in neonatal mouse hearts show potential for expansion and differentiation into CMs under conducive *in vitro* conditions (Laugwitz, 2005). Given that ISL1 transcriptionally governs the expression of a suite of cardiac genes, such as *NKX2-5* (Ma et al., 2008), *FGF10* (Watanabe et al., 2012), which are essential for embryonic cardiogenesis, inducing ISL1 expression in CMs could be a critical determinant in the induction of cells possessing regenerative capacity.

Aiming to replicate this regenerative capacity, our study focused on identifying small molecules capable of inducing ISL1 expression in CMs. Through a combinatorial screening approach, we discovered a novel combination of CHIR99021 and A-485, or 2C, that efficiently and unprecedentedly induces dedifferentiation of human CMs into RCCs. These RCCs exhibited disassembled sarcomeric structures, high expression of embryonic cardiogenic genes, and an increased number of CMs through re-differentiation *in vitro*. Further investigations showed that 2C robustly generates RCCs in adult mouse hearts and improves cardiac function in mice experiencing myocardial infarction. This proof-of-concept discovery demonstrates that a simple combination of small molecule drugs can endow the mammalian heart with regenerative capacity by reprogramming CMs into RCCs.

### Efficient induction of dedifferentiation in hESC-derived CMs by 2C treatment

To obtain an adequate number of CMs for small molecule screening, we differentiated hESCs into CMs (Movie 1, Figure 1—figure supplement 1A) following a well-established step-wise protocol (Lian et al., 2013). Nearly homogeneous contracting CMs were observed on day 10 of differentiation, consistent with previous reports. After purification with glucose-depleted medium containing abundant lactate (Figure 1—figure supplement 1B), highly pure TNNT2$^+$ CMs were obtained. These were subsequently dissociated and seeded into 96-well plates. Once the CMs resumed contraction, they were treated with individual small molecules from a collection of over 4,000 compounds for 3 days (Figure 1—figure supplement 1C), and then fixed and immunostained for ISL1. Using a high-content imaging (HCI) and analysis system, five compounds were initially identified as potential inducers of dedifferentiation in CMs, indicated by induced

sarcomere disassembly and ISL1 expression (Figure 1—figure supplement 1D). Further comparison revealed that the unique combination of CHIR99021 and A-485 (2C) most efficiently induced ISL1 expression in TNNT2$^+$ CMs (Figure 1—figure supplement 1E). Notably, while A-485 was screened at a concentration of 10 μM, its optimal working concentration in subsequent experiments was determined to be 0.5 μM based on titration experiments (Figure 1—figure supplement 1F-G). Of note, compound I-BET-762 also showed some capacity to induce ISL1 expression. However, it was less effective than A-485 in combination with CHIR99021 (Figure 1—figure supplement 1H).

When CMs with well-organized sarcomeres were treated with 2C *in vitro*, cells started to exhibit a dedifferentiation-associated phenotype, such as reduction of cell size after 24 hours, growing as clusters after 48 hours, and forming colonies after 60 hours (Figure 1A and Figure 1—figure supplement 2A). During this period, the expression of TNNT2 and MYL2 gradually downregulated while ISL1 expression and the percentage of ISL1$^+$ cells increased (Figure 1—figure supplement 2B). Compared to untreated CMs, significant sarcomere disassembly and reduction of cytoplasmic/nuclear area were observed in cells treated with 2C for 60 hours (Figure 1B-C). In parallel, the number and percentage of TNNT2$^+$ cells remained constant while ISL1$^+$ cells increased remarkably (Figure 1D-E and Figure 1—figure supplement 2C), accompanied by a ~3-fold increase in ISL1 expression at both mRNA and protein levels (Figure 1F and Figure 1—figure supplement 2B). Other early embryonic cardiogenesis genes, including MESP1, LEF1 (Klaus et al., 2007), FUT4 (Wang et al., 2019), and NR2F2 (Churko et al., 2018), were also highly expressed following 2C treatment (Figure 1G and Figure 1—figure supplement 2D). Furthermore, 2C treatment significantly decreased the expression of CM-specific genes, such as TNNT2, MYL2, MYL7, and MEF2C, while pan-cardiac transcription factors GATA4, TBX5, and NKX2-5 showed less effect (Figure 1G and Figure 1—figure supplement 2D). Notably, 2C induced ISL1 expression even in mature CMs derived from hESCs treated with ZLN005 (Liu et al., 2020) (Figure 1—figure supplement 2E). These results indicate that 2C treatment effectively reprograms CMs towards a dedifferentiated, embryonic-like state.

**2C induced cells possess regenerative capacity**

To confirm the regenerative capacity of 2C-induced cardiac cells, we investigated cell proliferation using a BrdU incorporation assay. Immunostaining showed the co-localization of ISL1 and BrdU labeling in these cells (Figure 2A). Statistical analysis revealed a significant decrease in the nuclear area and an increase in the number of ISL1$^+$/BrdU$^+$ positive cells following 2C treatment (Figure 2B-C). We then examined the potential for re-differentiation of 2C-induced cardiac cells into CMs. As expected, upon withdrawal of 2C and subsequent culture in CM media for 3 days (60h+3d), we observed the emergence of spontaneously contracting cells exhibiting CM-specific morphology and typical cytoplasmic/nuclear area size (Movie 2 and Figure 2D-E). These cells downregulated early embryonic cardiogenesis genes and upregulated CM-specific genes, with no noticeable changes in pan-cardiac genes (Figure 2—figure supplement 1A). Remarkably, there was a notable increase (roughly 1.4-fold) in the number of re-differentiated CMs with clear TNNT2 staining relative to the initial CMs before 2C treatment (Figure 2F), demonstrating the regenerative potential in 2C-induced cardiac cells. Additionally, 2C-induced cardiac cells could differentiate

104 into SMA$^+$ SMCs or CD31$^+$/VE-Cadherin$^+$ ECs in the presence of PDGF-BB and TGF-β1 or VEGF, bFGF
105 and BMP4, respectively (Figure 2G-H and Figure 2—figure supplement 1B). In contrast, these genes
106 expressed were not detectable in DMSO-treated cells. Collectively, our findings indicate that 2C treatment
107 facilitates the conversion of CMs into cardiac cells with regenerative capability, including proliferative
108 potential and differentiation into the three major cardiovascular cell types, thus named regenerative cardiac
109 cells (RCCs).

110 **Lineage tracing demonstrated that 2C induced RCCs dedifferentiated from TNNT2$^+$ CMs**

111 Although TNNT2$^+$ CMs purified using a lactate-based culture medium were nearly homogeneous
112 populations, a small fraction (<4%) of purified cells still expressing ISL1 (Figure 1—figure supplement 1B).
113 To ascertain that the RCCs induced by 2C treatment were indeed dedifferentiated from TNNT2$^+$ CMs rather
114 than originating from the proliferation of residual ISL1$^+$ cells, we conducted lineage-tracing experiments.
115 Using an ISL1$^{mCherry/+}$ H9 hESC (K9) line established through CRISPR-based knock-in (Figure 3—figure
116 supplement 1A-D), we verified that mCherry expression accurately mirrored endogenous ISL1 expression
117 (Figure 3A-C). Following the purification of K9-derived CMs and the selection of mCherry-negative cells by
118 FACS (Figure 3D-E), these cells were confirmed to be TNNT2$^+$ CMs (Figure 3—figure supplement 1E).
119 Upon treatment of these mCherry-negative CMs with 2C for 60 hours, we observed remarkable
120 morphological changes in mCherry$^+$/ISL1$^+$ RCCs compared to mCherry$^-$/TNNT2$^+$ CMs (Figure 3F),
121 accompanied by a dramatic downregulation of TNNT2 and MYL2 expression and a notable upregulation of
122 ISL1 and mCherry expression (Figure 3G). FACS analysis further validated that 2C could convert K9-
123 derived mCherry-negative CMs into mCherry$^+$/ISL1$^+$ cells (Figure 3H-I). Similar findings were obtained
124 using the HUES7 hESC line with an ISL1-mCherry knock-in reporter (K7) (Figure 3—figure supplement 2),
125 robustly demonstrating that 2C induces ISL1 expression in TNNT2$^+$ CMs, effectively generating RCCs.

126 Additionally, we used a lineage-tracing system to unequivocally confirm the conversion of CMs to
127 ISL1-expressing RCCs by 2C treatment. In this assay, CMs were transfected with plasmids encoding
128 CreERT2 under the control of the TNNT2 promoter and an EGFP reporter following a flox-stop-flox cassette
129 (Figure 3—figure supplement 3A). After optimizing viral titers and infection timing (Figure 3—figure
130 supplement 3B-D), approximately 0.6% of K9-derived mCherry-negative CMs were permanently labeled
131 with EGFP following 6 days of tamoxifen treatment (Figure 3J-K). These EGFP-labeled mCherry-negative
132 CMs were then sorted by flow cytometry and treated with 2C for 60 hours. As expected, ISL1 expression
133 was observed in these EGFP$^+$ CMs (Figure 3L). Collectively, these results strongly indicate that the RCCs
134 with ISL1 expression were genuinely generated by 2C treatment from TNNT2$^+$ CMs.

135 **2C-induced dedifferentiation of CMs provided a protective effect on cardiac infarction**

136 To examine the reprogramming effect of 2C on CMs *in vivo*, we first tested 2C on primary neonatal rat CMs
137 (Sakurai et al., 2014), which consistently induced RCC generation with corresponding ISL1 induction and
138 morphological changes (Figure 4—figure supplement 1A). We then evaluated whether 2C could reprogram
139 endogenous CMs to RCCs *in vivo*. Neonatal SD rats were intraperitoneally administrated 20 mg/kg of

140 CHIR99021 and 10 mg/kg of A-485 daily for 5 days (Figure 4—figure supplement 1B). Compared to the
141 vehicle/DMSO controls (NC), ISL1 was robustly induced in the CMs of rats treated with 2C without apparent
142 effects on heart to body weight ratio (Figure 4—figure supplement 1C-D). These induced ISL1-expressing
143 cells were widely distributed within the region 600 μm to 3000 μm down from the base of the hearts,
144 including the aorta (Ao), left/right atria, and both ventricles (Figure 4—figure supplement 1E). All these
145 $ISL1^+$ cells also expressed TNNT2, indicating that 2C-induced RCCs originated from CMs *in vivo*.
146 Importantly, neither CHIR99021 nor A-485 alone induced $ISL1^+$ cells in ventricles, highlighting the combined
147 effect of 2C on RCC induction (Figure 4—figure supplement 2).

148 Similarly, RCCs were efficiently induced in the Ao root and RA regions of the heart dissected from
149 adult 129SvJ mice administrated 2C (20 mg/kg of CHIR99021 and 10 mg/kg of A-485) for 5 consecutive
150 days (Figure 4A). To explore whether 2C-induced RCCs could rescue cardiac function in mice subjected
151 to myocardial infarction (MI), we conducted both prophylactic and therapeutic studies. In the prophylactic
152 setting, mice were pre-treated with either 2C or vehicle/DMSO for 5 days (Figure 4B) before inducing MI by
153 ligation of left anterior descending (LAD) artery. When measuring cardiac function with magnetic resonance
154 imaging (MRI) on days 1, 8, 25 and 35 post-MI, we found pretreatment with 2C significantly improved both
155 cardiac function and survival rate without affecting body weight (Figure 4C-E). In the therapeutic setting
156 (Figure 4F), mice treated with 2C post-MI displayed recovered cardiac function as assessed by left
157 ventricular ejection fraction (LVEF) and echocardiography (Figure 4G-H). Cardiac fibrosis was largely
158 ameliorated in 2C-treated mice, displaying significantly smaller scar sizes compared to control mice (Figure
159 4I). Altogether, these *in vivo* studies collectively indicate that 2C-induced RCCs possess regenerative
160 capacities comparable to those generated *in vitro,* shedding light on the development of small molecule
161 drugs with similar mechanisms for therapeutic use in repairing or regenerating hearts after cardiac injury.

162 **Dedifferentiation requirement of CHIR99021 and A-485**

163 To elucidate the mechanisms behind the in 2C-induced dedifferentiation of CMs into RCCs, we performed
164 bulk RNA-seq on K9-derived ISL1/mCherry-negative CMs treated with either DMSO as a negative control
165 (NC) or the 2C combination for 60 hours (Figure 5A). Analysis of differentially expressed genes (DEGs)
166 revealed substantial transcriptomic alterations; specifically, 2C treatment upregulated embryonic
167 cardiogenesis genes such as MSX1, BMP4, TCF4, and LEF1, and downregulated genes associated with
168 CMs (Figure 5B-C). Gene ontology (GO) analysis further indicated a suppression of genes involved in
169 cardiac maturation and muscle contraction, contrasting with an enrichment in genes part of the catenin
170 complex (Figure 5D-F). These findings were corroborated by qPCR, confirming the significant up-regulation
171 of embryonic genes (e.g., MSX2, NKD1, PDGFC, CTNNA2) in K9-derived mCherry-negative CMs (Figure
172 5G).

173 We investigated the individual and combined effects of CHIR99021 and A-485 on inducing RCC
174 characteristics. Morphological assessments showed that CHIR99021 significantly reduced both
175 cytoplasmic and nuclear areas—a feature characteristic of RCCs—more effectively than A-485, which
176 primarily reduced cytoplasmic area only (Figure 5—figure supplement 1A-C). Sarcomere disassembly was

more pronounced with CHIR99021 treatment, aligning with its role in enhancing embryonic cardiogenesis genes like BMP4 and LEF1 (Figure 5—figure supplement 1D-E). A-485, while not affecting the nuclear area to the same extent, played a crucial role in the epigenetic reprogramming of CMs. It facilitated the suppression of CM-specific genes, such as TNNT2, through epigenetic modifications, enhancing the expression of RCC-specific genes such as ISL1 in conjunction with CHIR99021 (Figure 5—figure supplement 1D). This indicates that while CHIR99021 drives the initial dedifferentiation process by altering the cellular morphology and gene expression associated with embryonic cardiogenesis, A-485 enhances these effects by providing necessary epigenetic conditions for sustaining and stabilizing the RCC phenotype. Despite both compounds independently inducing reduced expression of TNNT2 and MYL2, as well as increased ISL1 expression, CHIR99021 uniquely influences a cohort involved in embryonic cardiogenesis, including BMP4, NKD1, MSX2, PDGFC, LEF1, and TCF4 (Figure 5—figure supplement 1D). Upon withdrawal of CHIR99021, A-485 or 2C, the cell percentage of $ISL1^{+}$ cell was similarly and significantly reduced (Figure 5—figure supplement 1F). Notably, a drastic increase in the number of $TNNT2^{+}$ CMs was observed only during the redifferentiation of 2C-treated cells, as confirmed by statistical analysis (Figure 5—figure supplement 1G). These findings suggest that while CHIR99021 plays a leading role in 2C-induced de-differentiation of CMs to RCCs, A-485 is also indispensable, particularly in modifying the epigenetic landscape to support the transition and maintenance of reprogrammed state.

**Reprogramming of CMs to RCCs by 2C went through an intermediate cell state**

In the exploration of CM reprogramming to RCC using 2C treatment, single-cell RNA sequencing (scRNA-seq) was utilized to trace the progression through distinct cellular states of K9-derived mCherry-negative CMs treated with either DMSO (NC) or the 2C for 60 hours. Through UMAP analysis, we identified seven distinct clusters, observing notable increases in the proportions of cells in clusters 0, 2 and 3 following 2C treatment (Figure 6A-B). Cells within cluster 2 prominently expressed genes characteristic of RCCs, such as ISL1, BMP4 and FGF20—a gene crucial for the expansion of early embryonic progenitor cells (Cohen et al., 2007)), along with the cell proliferation marker MKI67 (Figure 6C-D). This distinct expression pattern marked them as transitioning towards an RCC phenotype. In contrast, clusters 0, 3, 4, and 5 maintained high expression levels of CM-specific markers like MYH6 and MYL2 (Figure 6C-D), indicating their retention of a mature CM identity. Interestingly, cells in clusters 1 and 6 exhibited characteristics of intermediate cells (ICs), expressing both dedifferentiation markers such as ACTA2 and genes linked to CM development, including COL1A1, COL1A2, and COL3A1 (Cui et al., 2020; Mononen et al., 2020) (Figure 6C-D). This highlighted these clusters as transitional states in the reprogramming process from CMs to RCCs.

Further detailed analysis of cluster 2, comparing 435 cells from DMSO-treated samples with 410 cells from 2C-treated samples, allowed us to identify a prominent subcluster (subcluster 0) comprising 408 cells (48.3% of the cluster), exclusively found in 2C-treated samples (Figure 6E-F). Cells in this subcluster were defined by high expression of key embryonic cardiogenesis genes such as MSX1, LEF1, BMP4, MSX2, and HAND1, along with genes typically co-expressed with ISL1 in SHF progenitors, including NR2F2, TBX5, ALCAM (Ghazizadeh et al., 2018), and CXCR4 (Andersen et al., 2018) (Figure 6G). This specific

214 gene expression profile robustly indicates that the cells in subcluster 0 have adopted an RCC identity,
215 indicative of successful induction by 2C treatment. Thus, a unique gene set that included LIX1, NKD1,
216 PDGFC, ARL4A, AXIN2, FZD7, ISL1, MSX1, MSX2, BMP4, LEF1, and HAND1 was found to determine
217 RCC state during the reprogramming of CMs by 2C, and hence designated as RCC genes.

218 To further quantify this transition, pseudo-time analysis was performed, clearly delineating the 2C-
219 induced reprogramming trajectory from CMs, highly expressing TNNT2, through ICs, characterized by the
220 expression of COL1A1, to RCCs, marked by elevated levels of ISL1 and FGF20) (Figure 6H-J). This
221 analysis confirms the dynamic and stepwise nature of cellular transformation under 2C treatment.

222 **Epigenetic regulation of CMs and RCCs genes by 2C treatment**

223 As previously documented (Lasko et al., 2017), A-485 functions as a p300 acetyltransferase inhibitor,
224 specifically reducing acetylation at lysine 27 of histone H3 (H3K27Ac), but not at lysine 9 (H3K9Ac), as
225 shown in studies with PC3 cells. Our data corroborate these findings, showing a notable decrease in
226 H3K27Ac levels in CMs treated with A-485 alone, while levels of H3K9Ac remain unaffected (Figure 7—
227 figure supplement 1A-E). However, treatment with CHIR99021 or the combined 2C regime did not
228 significantly alter the acetylation patterns of these histone marks (Figure 7—figure supplement 1).
229 Intriguingly, we observed that although the number of H3K9Ac$^+$ cells remained unchanged in CMs, the
230 fluorescence intensity was significantly decreased after A-485 treatment (Figure 7—figure supplement 1F),
231 suggesting a distinctive regulatory role of A-485 in modulating histone acetylation in CM reprogramming.

232 To explore the molecular mechanisms by which the 2C treatment modulates gene expression during
233 the reprogramming of hESC-derived CMs into RCCs, we conducted chromatin immunoprecipitation
234 followed by sequencing (ChIP-seq) analyses. This study focused on H3K27Ac and H3K9Ac modifications
235 across various treatment conditions (Figure 7A). Our analysis identified regions near transcription start sites
236 (±4 kb) that were rich in H3K4me3, indicative of active promoters in both control (DMSO-treated) and 2C-
237 treated cells (Figure 7B-C). Following 2C treatment, there was a marked increase in H3K9Ac and H3K27Ac
238 levels around the transcription start sites (TSS), suggesting enhanced gene activity. Specifically, 2C
239 treatment significantly increased H3K9Ac enrichment at 4,485 gene promoters and H3K27Ac at 2,560 gene
240 promoters, with corresponding decreases in 346 and 1,834 genes, respectively (Figure 7—figure
241 supplement 2A-F). Notably, genes that showed reduced acetylation in response to A-485 also displayed
242 similar trends under 2C treatment, highlighting genes with functions crucial to cardiac muscle activity such
243 as contraction and sarcomere organization (Figure 7—figure supplement 2). In comparison with treatments
244 using A-485 or CHIR99021 alone, the 2C combination notably augmented acetylation at genes involved in
245 cell cycle regulation and cell division, suggesting a synergistic effect of the dual treatment in promoting
246 gene activation essential for cardiac regeneration (Figure 7—figure supplement 2).

247 We also specifically analyzed the acetylation peaks at promoters of key CM genes and RCC genes.
248 A-485 treatment predominantly decreased H3K9Ac and H3K27Ac peaks at CM gene promoters such as
249 TNNT2, TNNI1, MYL7, MYH6, and MYH7, aiding their downregulation. These reductions were intensified

250 under 2C treatment, reflecting its potent effect in repressing mature cardiomyocyte markers while activating
251 regenerative pathways (Figure 7D and Figure 7—figure supplement 3). In contrast, CHIR99021 effectively
252 upregulated H3K9Ac and H3K27Ac at promoters of the RCC genes such as LEF1, AXIN2, BMP4, LIX1,
253 MSX1, MSX2, and NKD1, with 2C treatment further enhancing these effects, confirming its robust impact
254 on inducing a regenerative phenotype in treated cells (Figure 7D and Figure 7—figure supplement 3).

255 Moreover, the distribution of H3K9Ac and H3K27Ac changes during 2C-induced dedifferentiation
256 revealed that these modifications are more dynamically associated with H3K9Ac, particularly in the
257 transition of CMs to RCCS. This dynamic regulation was illustrated by the significant number of genes
258 showing exclusive enrichment under 2C treatment compared to control or single-drug treatments (Figure
259 7E-F). In detail, of genes with H3K9Ac enrichment, 2716 (or 46.1%) out of 5891 annotated genes were only
260 enriched in the cells treated with 2C, while only 527 (or 4.9%) out of 10785 annotated genes with H3K27Ac
261 enrichment were exclusively observed (Figure 7E-F). To further confirm this notion, we performed a
262 comparative analysis of annotated genes between the cells treated with 2C or DMSO to validate the most
263 significant differential genes (i.e., Log10LR>3) under the respective condition. In comparison to 430 genes
264 with H3K9Ac enrichment observed in DMSO-treated cells, which were mainly involved in cardiac muscle
265 contraction (Figure 7G-H), 2C treatment markedly enhanced the enrichment of H3K9Ac in 123 genes
266 associated with the transcription factor complex and Wnt signaling pathway (Figure 7I-J). In particular, 12
267 CM genes, including TNNT2, were ranked in the top 90 out of 430 annotated genes with H3K9Ac
268 enrichment. In contrast, 7 RCC genes, including ISL1, were ranked in the top 50 out of 123 annotated
269 genes with H3K9Ac enrichment.

270 Lastly, our findings were substantiated by DNA-binding motif analyses, which showed increased
271 accessibility of ISL1 binding sites only in cells treated with A-485 or the 2C combination, underscoring the
272 critical role of A-485 in activating RCCs genes through ISL1-dependent mechanisms (Figure 7K).
273 Collectively, these results underscore the efficiency of combining CHIR99021 and A-485 in reprogramming
274 CMs to RCCs, opening new avenues for developing therapies aimed at cardiac regeneration.

275 **Discussion**

276 The generation of regenerative cardiac cells (RCCs) from cardiomyocytes (CMs) using the 2C treatment, a
277 combination of CHIR99021 and A-485, represents a significant advancement in cardiac regenerative
278 medicine. This study demonstrates that the synergistic interaction between these two molecules is essential
279 for the reprogramming of endogenous CMs into RCCs, as evidenced by the absence of RCCs in postnatal
280 rat hearts treated with either molecule alone (Figure 4—figure supplement 2). CHIR99021, a well-
281 documented GSK3 inhibitor, activates the Wnt signaling pathway, thereby promoting the proliferation of
282 human pluripotent stem cell-derived CMs (Buikema et al., 2020; Quaife-Ryan et al., 2020). It also induces
283 H3K27Ac at promoters of critical cardiac genes such as TNNT2, MYH6, and ISL1 (Quaife-Ryan et al.,
284 2020). This observation aligns with our findings, which show a slight increase H3K27Ac levels in CMs
285 following CHIR99021 treatment (Figure 7D and Figure 7—figure supplement 1). Moreover, our results
286 reveal that the p300/CBP inhibitor A-485 facilitates CM dedifferentiation into RCCs by epigenetically

287 suppressing CM-specific gene expression (Figure 7D), consistent with a decline in the fluorescence
288 intensity of H3K27Ac and H3K9Ac in CMs (Figure 7—figure supplement 1C and E). Concurrently A-485
289 enhances modifications conducive to the RCC state, such as H3K9Ac and H3K27Ac on genes like ISL1
290 (Figure 7D). This dual mechanism of action underscores the potential of utilizing epigenetic modifiers like
291 A-485 to influence cell fate decisions in terminally differentiated cells, suggesting broader applications in
292 regenerative biology.

293 The RCCs induced by the 2C treatment not only re-expressed genes essential for embryonic
294 cardiogenesis but also demonstrated the capability to differentiate into three cardiac lineages *in vitro*,
295 mirroring the properties of $ISL1^+$ second heart field cardiac progenitors (Bu et al., 2009; Moretti et al., 2006).
296 Although these 2C-induced RCCs show limited proliferation compared to natural $ISL1^+$ progenitors, their
297 potential for expansion under defined conditions presents an intriguing avenue for future research. These
298 insights contribute significantly to the understanding of cardiac lineage plasticity and highlight the
299 therapeutic potential of induced multipotent cardiovascular progenitors for heart repair and regeneration.

300 Despite these promising findings, several limitations warrant further investigation. The modest
301 proliferation ability of 2C-induced RCCs relative to natural cardiac progenitors suggests that optimizing the
302 culture conditions or treatment protocols may enhance their regenerative capacity. Additionally, the specific
303 molecular mechanisms through which CHIR99021 and A-485 synergistically promote RCC formation
304 remain incompletely understood. Future studies should aim to delineate these pathways more clearly,
305 potentially through *in vivo* lineage tracing to map the fate decisions of individual cells. Moreover, the
306 potential off-target effects of 2C treatment and its long-term impacts on cardiac function and structure need
307 comprehensive evaluation. As we advance, exploring the scalability of this approach and its applicability to
308 other types of terminally differentiated cells could broaden the scope of regenerative therapies, offering new
309 strategies for numerous degenerative conditions. In conclusion, this study not only sheds light on the
310 cellular and molecular intricacies of cardiac cell dedifferentiation but also opens new pathways for the
311 development of regenerative therapies aimed at heart disease.

312 **References**


313 Andersen, P., Tampakakis, E., Jimenez, D. V., Kannan, S., Miyamoto, M., Shin, H. K., Saberi,
314 A., Murphy, S., Sulistio, E., Chelko, S. P., & Kwon, C. (2018). Precardiac organoids
315 form two heart fields via Bmp/Wnt signaling. *Nat Commun*, *9*(1), 3140.
316 https://doi.org/10.1038/s41467-018-05604-8
317 Bu, L., Jiang, X., Martin-Puig, S., Caron, L., Zhu, S., Shao, Y., Roberts, D. J., Huang, P. L.,
318 Domian, I. J., & Chien, K. R. (2009). Human ISL1 heart progenitors generate diverse
319 multipotent cardiovascular cell lineages. *Nature*, *460*(7251), 113-117.
320 https://doi.org/10.1038/nature08191
321 Buikema, J. W., Lee, S., Goodyer, W. R., Maas, R. G., Chirikian, O., Li, G., Miao, Y., Paige, S.
322 L., Lee, D., Wu, H., Paik, D. T., Rhee, S., Tian, L., Galdos, F. X., Puluca, N., Beyersdorf,
323 B., Hu, J., Beck, A., Venkamatran, S., . . . Wu, S. M. (2020). Wnt Activation and
324 Reduced Cell-Cell Contact Synergistically Induce Massive Expansion of Functional
325 Human iPSC-Derived Cardiomyocytes. *Cell Stem Cell*, *27*(1), 50-63 e55.
326 https://doi.org/10.1016/j.stem.2020.06.001
327 Churko, J. M., Garg, P., Treutlein, B., Venkatasubramanian, M., Wu, H., Lee, J., Wessells, Q.
328 N., Chen, S. Y., Chen, W. Y., Chetal, K., Mantalas, G., Neff, N., Jabart, E., Sharma, A.,
329 Nolan, G. P., Salomonis, N., & Wu, J. C. (2018). Defining human cardiac transcription
330 factor hierarchies using integrated single-cell heterogeneity analysis. *Nat Commun*, *9*(1),
331 4906. https://doi.org/10.1038/s41467-018-07333-4
332 Cohen, E. D., Wang, Z., Lepore, J. J., Lu, M. M., Taketo, M. M., Epstein, D. J., & Morrisey, E.
333 E. (2007). Wnt/beta-catenin signaling promotes expansion of Isl-1-positive cardiac
334 progenitor cells through regulation of FGF signaling. *J Clin Invest*, *117*(7), 1794-1804.
335 https://doi.org/10.1172/JCI31731
336 Cui, M., Wang, Z., Chen, K., Shah, A. M., Tan, W., Duan, L., Sanchez-Ortiz, E., Li, H., Xu, L.,
337 Liu, N., Bassel-Duby, R., & Olson, E. N. (2020). Dynamic Transcriptional Responses to
338 Injury of Regenerative and Non-regenerative Cardiomyocytes Revealed by Single-
339 Nucleus RNA Sequencing. *Developmental Cell*, *53*(1), 102-116.e108.
340 https://doi.org/10.1016/j.devcel.2020.02.019
341 Ghazizadeh, Z., Fattahi, F., Mirzaei, M., Bayersaikhan, D., Lee, J., Chae, S., Hwang, D., Byun,
342 K., Tabar, M. S., Taleahmad, S., Mirshahvaladi, S., Shabani, P., Fonoudi, H., Haynes, P.
343 A., Baharvand, H., Aghdami, N., Evans, T., Lee, B., & Salekdeh, G. H. (2018).
344 Prospective Isolation of ISL1(+) Cardiac Progenitors from Human ESCs for Myocardial
345 Infarction Therapy. *Stem Cell Reports*, *10*(3), 848-859.
346 https://doi.org/10.1016/j.stemcr.2018.01.037
347 Kikuchi, K., & Poss, K. D. (2010). Primary contribution to zebrafish heart regeneration by
348 gata4(+) cardiomyocytes. *Nature*, *464*(7288), 601-605.
349 https://doi.org/10.1038/nature08804
350 Klaus, A., Saga, Y., Taketo, M. M., Tzahor, E., & Birchmeier, W. (2007). Distinct roles of
351 Wnt/beta-catenin and Bmp signaling during early cardiogenesis. *Proc Natl Acad Sci U S*
352 *A*, *104*(47), 18531-18536. https://doi.org/10.1073/pnas.0703113104
353 Lasko, L. M., Jakob, C. G., Edalji, R. P., Qiu, W., Montgomery, D., Digiammarino, E. L.,
354 Hansen, T. M., Risi, R. M., Frey, R., Manaves, V., Shaw, B., Algire, M., Hessler, P.,
355 Lam, L. T., Uziel, T., Faivre, E., Ferguson, D., Buchanan, F. G., Martin, R. L., . . .
356 Bromberg, K. D. (2017). Discovery of a selective catalytic p300/CBP inhibitor that
357 targets lineage-specific tumours. *Nature*, *550*(7674), 128-132.
358 https://doi.org/10.1038/nature24028

359 Laugwitz, K.-L. (2005). Postnatal isl1 cardioblasts enter fully differentiated cardiomyocyte
360 lineages. *Nature*.
361 Lepilina, A., Coon, A. N., Kikuchi, K., Holdway, J. E., Roberts, R. W., Burns, C. G., & Poss, K.
362 D. (2006). A dynamic epicardial injury response supports progenitor cell activity during
363 zebrafish heart regeneration. *cell*, *127*(3), 607-619.
364 https://doi.org/10.1016/j.cell.2006.08.052
365 Lian, X., Zhang, J., Azarin, S. M., Zhu, K., Hazeltine, L. B., Bao, X., Hsiao, C., Kamp, T. J., &
366 Palecek, S. P. (2013). Directed cardiomyocyte differentiation from human pluripotent
367 stem cells by modulating Wnt/beta-catenin signaling under fully defined conditions. *Nat*
368 *Protoc*, *8*(1), 162-175. https://doi.org/10.1038/nprot.2012.150
369 Liu, Y., Bai, H., Guo, F., Thai, P. N., Luo, X., Zhang, P., Yang, C., Feng, X., Zhu, D., Guo, J.,
370 Liang, P., Xu, Z., Yang, H., & Lu, X. (2020). PGC-1alpha activator ZLN005 promotes
371 maturation of cardiomyocytes derived from human embryonic stem cells. *Aging (Albany*
372 *NY)*, *12*(8), 7411-7430. https://doi.org/10.18632/aging.103088
373 Ma, Q., Zhou, B., & Pu, W. T. (2008). Reassessment of Isl1 and Nkx2-5 cardiac fate maps using
374 a Gata4-based reporter of Cre activity. *Dev Biol*, *323*(1), 98-104.
375 https://doi.org/10.1016/j.ydbio.2008.08.013
376 Mononen, M. M., Leung, C. Y., Xu, J., & Chien, K. R. (2020). Trajectory mapping of human
377 embryonic stem cell cardiogenesis reveals lineage branch points and an ISL1 progenitor-
378 derived cardiac fibroblast lineage. *Stem Cells*. https://doi.org/10.1002/stem.3236
379 Moretti, A., Caron, L., Nakano, A., Lam, J. T., Bernshausen, A., Chen, Y., Qyang, Y., Bu, L.,
380 Sasaki, M., Martin-Puig, S., Sun, Y., Evans, S. M., Laugwitz, K. L., & Chien, K. R.
381 (2006). Multipotent embryonic isl1+ progenitor cells lead to cardiac, smooth muscle, and
382 endothelial cell diversification. *cell*, *127*(6), 1151-1165.
383 https://doi.org/10.1016/j.cell.2006.10.029
384 Porrello, E. R., Mahmoud, A. I., Simpson, E., Hill, J. A., Richardson, J. A., Olson, E. N., &
385 Sadek, H. A. (2011). Transient regenerative potential of the neonatal mouse heart.
386 *Science*, *331*(6020), 1078-1080. https://doi.org/10.1126/science.1200708
387 Quaife-Ryan, G. A., Mills, R. J., Lavers, G., Voges, H. K., Vivien, C. J., Elliott, D. A.,
388 Ramialison, M., Hudson, J. E., & Porrello, E. R. (2020). beta-Catenin drives distinct
389 transcriptional networks in proliferative and nonproliferative cardiomyocytes.
390 *Development*, *147*(22). https://doi.org/10.1242/dev.193417
391 Sakurai, T., Lanahan, A., Woolls, M. J., Li, N., Tirziu, D., & Murakami, M. (2014). Live cell
392 imaging of primary rat neonatal cardiomyocytes following adenoviral and lentiviral
393 transduction using confocal spinning disk microscopy. *J Vis Exp*(88), e51666.
394 https://doi.org/10.3791/51666
395 Srivastava, D. (2006). Making or breaking the heart: from lineage determination to
396 morphogenesis. *cell*, *126*(6), 1037-1048. https://doi.org/10.1016/j.cell.2006.09.003
397 Wang, J., Liu, M., Wu, Q., Li, Q., Gao, L., Jiang, Y., Deng, B., Huang, W., Bi, W., Chen, Z.,
398 Chin, Y. E., Paul, C., Wang, Y., & Yang, H. T. (2019). Human Embryonic Stem Cell-
399 Derived Cardiovascular Progenitors Repair Infarcted Hearts Through Modulation of
400 Macrophages via Activation of Signal Transducer and Activator of Transcription 6.
401 *Antioxid Redox Signal*, *31*(5), 369-386. https://doi.org/10.1089/ars.2018.7688
402 Watanabe, Y., Zaffran, S., Kuroiwa, A., Higuchi, H., Ogura, T., Harvey, R. P., Kelly, R. G., &
403 Buckingham, M. (2012). Fibroblast growth factor 10 gene regulation in the second heart
404 field by Tbx1, Nkx2-5, and Islet1 reveals a genetic switch for down-regulation in the

405 myocardium. *Proc Natl Acad Sci U S A*, *109*(45), 18273-18280.
406 https://doi.org/10.1073/pnas.1215360109
407

**Acknowledgments**

This work is supported by the National Natural Science Foundation of China (32030031 to S.D.), Beijing Natural Science Foundation (JQ22016 to T.M.), the National Key R&D Program of China (2022YFA1103704 to S.D.; 2022YFA1104503 to Y. N.), Center for Life Sciences (to S.D.).

We also thank the Center for Pharmaceutical Technology, Tsinghua University for the activity screening platform, Biomarker Technologies Corporation, Beijing, China and BeiJing Geek Gene Technology Co Ltd for technical support, and support from Tsinghua-Peking Center for Life Sciences.

**Author Contributions**

Conceptualization, S.D. and W.Z.; Methodology, W.Z., H.L., T.H.M. and Y.N.; Investigation, W.Z., C.Y.W., K.Z.H., P.Q.W., B.W.W., and H.G.; Visualization, W.Z., P.Q.W., B.W.W., H.G., and D.W.; Funding Acquisition, S.D., T.H.M., and Y.N.; Project Administration, W.Z., H.L., T.H.M., and Y.N.; Supervision: S.D., and W.Z.; Writing – Original Draft, W.Z., T.H.M., and S.D.; Writing – Review & Editing: W.Z., T.H.M., Y.N., S.D.

**Competing Interests**

The authors declare no competing interests.

**Data and Materials availability**

All targeted amplicon sequencing data have been deposited in the Sequence Read Archive of the NCBI under the BioProject accession number PRJNA903530. All data are available in the main text or the supplementary materials.

427 **Figure and Figure legends**

428 **Figure 1. 2C treatment induced dedifferentiation of hESC-derived CMs toward ISL1-expressing**
429 **cells.** Cells induced from hESC-derived CMs by treatment with DMSO (NC) or 2C for 60 hours. **(A)** Phase
430 contrast images showing cell morphology. **(B)** Immunofluorescence staining of the ISL1 (ISL1, green), and
431 the CM marker cardiac troponin T (TNNT2, red) in the cells. Nuclei were stained by DAPI (4′,6-diamidino-
432 2-phenylindole) and presented in DNA blue. **(C)**, Cytosolic and nuclear areas of the cells. Data are shown
433 as mean ± SD. (n=3 independent experiments, represented as dots). Two-way ANOVA with Dunnett's
434 multiple comparisons test. ****P < 0.0001. **(D)** Changes in cell number after 2C treatment. Total cell number,
435 $TNNT2^+$ cell number and $ISL1^+$ cell number were normalized to the negative control DMSO (NC). Data are
436 shown as mean ± SD (n=3 independent experiments, represented as dots). Two-way ANOVA with Šidák's
437 multiple comparisons test. ns, not significant (P > 0.05), ****P < 0.0001. **(E)** Fraction of $ISL1^+$ cells in
438 $TNNT2^+$ cells. Data are shown as mean ± SD (n=3 independent experiments, represented as dots). Two-
439 way ANOVA with Šidák's multiple comparisons test. **P < 0.01. **(F)** Western blot and quantitative analysis
440 of ISL1 expression in DMSO (NC) or 2C-treated CMs for 60 hours. Data are shown as mean ± SD. Unpaired
441 t test. *P < 0.05. **(G)** Relative gene expression of embryonic cardiogenesis marker genes (*MESP1*, *ISL1*,
442 *NR2F2*, *FUT4*, and *LEF1*), pan-cardiac genes (*GATA4*, *TBX5*, and *NXK2-5*), and CM marker genes
443 (*MEF2C*, *TNNT2*, *MYL2*, and *MYL7*) in the cells treated by DMSO (NC) or 2C for 60 hours (60h). Data are
444 shown as mean ± SD (n=3 independent experiments, represented as dots). Multiple unpaired t tests. ns,
445 not significant (P > 0.05), *P < 0.05, **P < 0.01, ***P < 0.001, ****P < 0.0001.

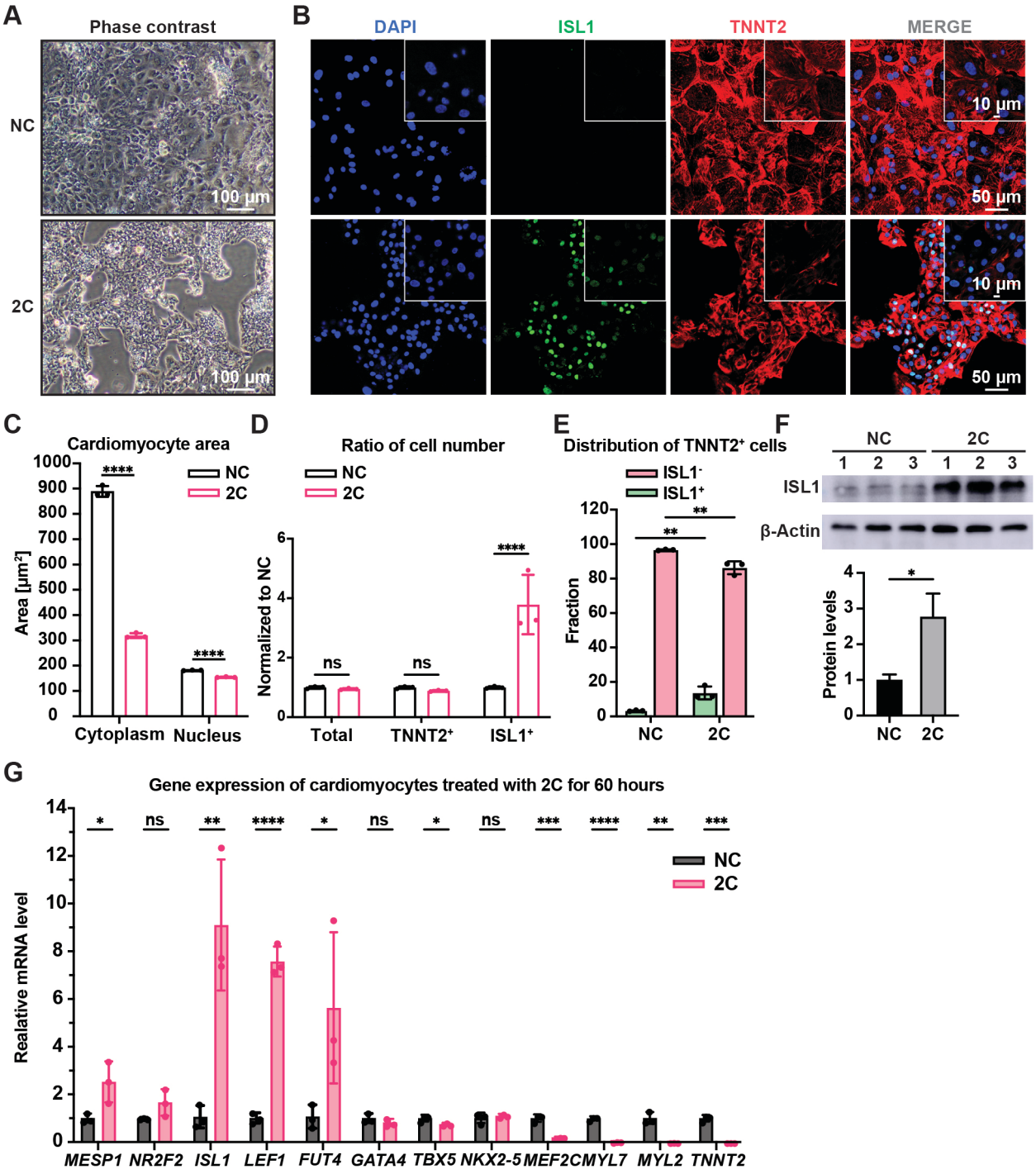
A
Phase contrast
NC
2C
100 μm
100 μm
B
DAPI
ISL1
TNNT2
MERGE
10 μm
50 μm
10 μm
50 μm
C
Cardiomyocyte area
NC
2C
Area [μm²]
Cytoplasm
Nucleus
D
Ratio of cell number
NC
2C
Normalized to NC
Total
TNNT2⁺
ISL1⁺
ns
E
Distribution of TNNT2⁺ cells
ISL1⁻
ISL1⁺
Fraction
NC
2C
F
NC
2C
ISL1
β-Actin
Protein levels
NC
2C
G
Gene expression of cardiomyocytes treated with 2C for 60 hours
NC
2C
Realative mRNA level
MESP1
NR2F2
ISL1
LEF1
FUT4
GATA4
TBX5
NKX2-5
MEF2C
MYL7
MYL2
TNNT2

446

447 **Figure 2. Regenerative ability of 2C-induced RCCs. (A-C)** Immunofluorescence staining (**A**) and
448 statistical analysis (**B** and **C**) of the ISL1 (green) and BrdU (red) double positive RCCs induced from CMs
449 by treatment with DMSO (NC) or 2C for 60 hours. The $ISL1^+$ cell number and $ISL1^+/BrdU^+$ cell number were
450 normalized to the negative control DMSO (NC). DAPI (4′,6-diamidino-2-phenylindole) staining labeled
451 nuclei as blue. Data are shown as mean ± SD (n=3 independent experiments, represented as dots). Multiple
452 unpaired t tests in (**B**), ****P < 0.0001. Two-way ANOVA with Šidák's multiple comparisons test in (**C**), **P
453 < 0.01, ****P < 0.0001. **(D)** Phase contrast images of hESC-derived CMs treated by DMSO (NC) or 2C for
454 60 hours (60h) and subsequently cultured in the absence of 2C for another 3 days (60h+3d). **(E)**
455 Immunostaining showed the expression of ISL1 (green) and TNNT2 (red) in the cells under the same
456 condition in (**D**). **(F)** Statistical analysis of $TNNT2^+$ cell numbers under the same condition in (**D**). Data are
457 shown as mean ± SD (n=3 independent experiments, represented as dots). Two-way ANOVA with Šidák's
458 multiple comparisons test. ns, not significant (P > 0.05), ****P < 0.0001. **(G)** Schematic diagram of directed
459 differentiation of 2C-induced RCCs towards cardiomyocytes (CMs), smooth muscle cells (SMCs) and
460 endothelial cells (ECs). **(H)** Immunostaining showed the expression of EC markers (CD31, green and
461 CD144, red), SMC marker (SMA, red), and CM marker (TNNT2, green). DAPI (4′,6-diamidino-2-
462 phenylindole) staining labeled nuclei as blue.

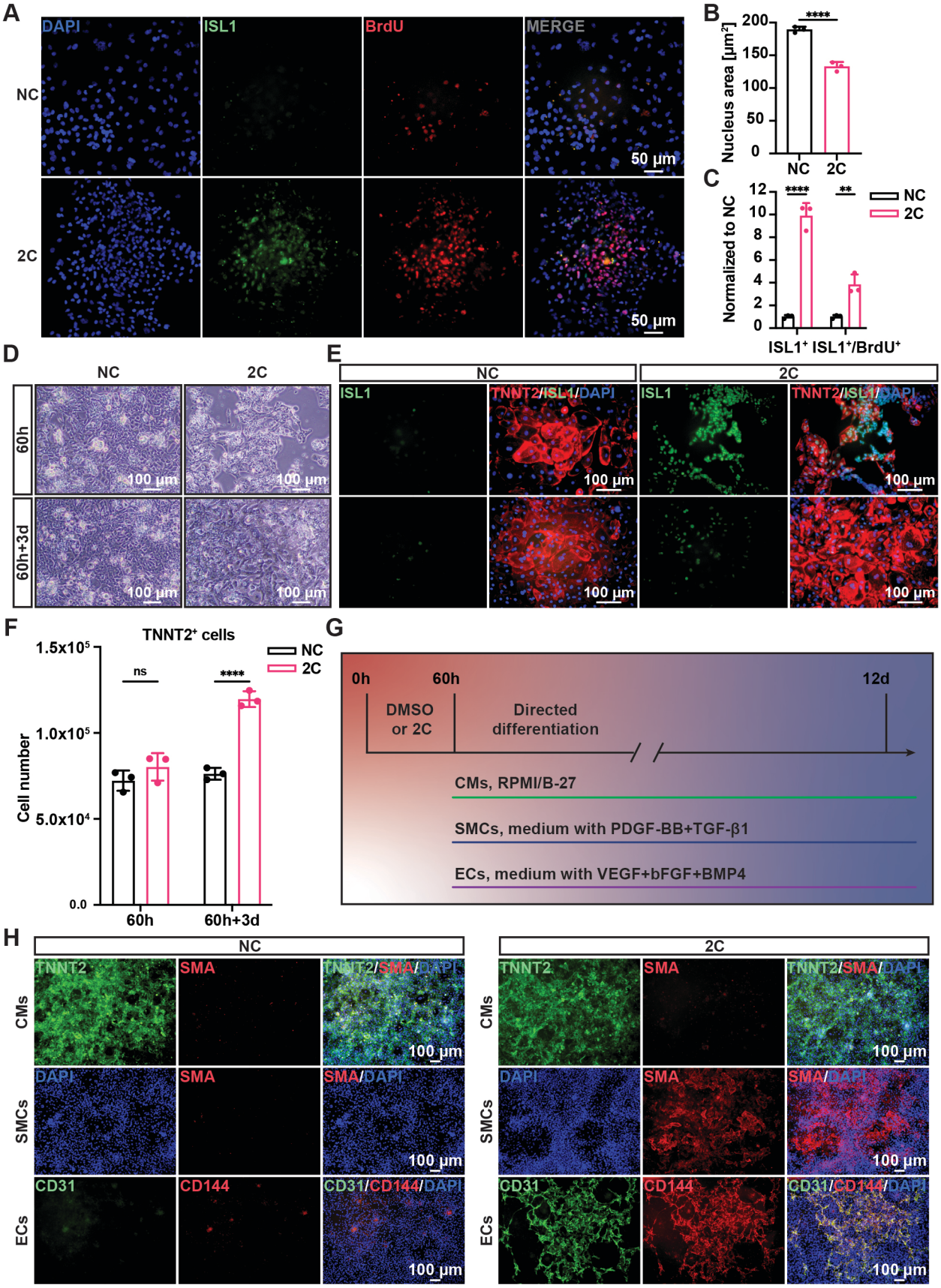
A
DAPI
ISL1
BrdU
MERGE
NC
2C
50 μm
B
Nucleus area [μm²]
200
150
100
50
0
****
NC
2C
C
Normalized to NC
12
10
8
6
4
2
0
****
**
NC
2C
ISL1⁺
ISL1⁺/BrdU⁺
D
NC
2C
60h
60h+3d
100 μm
E
NC
2C
ISL1
TNNT2/ISL1/DAPI
100 μm
F
TNNT2⁺ cells
1.5x10⁵
1.0x10⁵
5.0x10⁴
0.0
Cell number
ns
****
NC
2C
60h
60h+3d
G
0h
60h
12d
DMSO
or 2C
Directed
differentiation
CMs, RPMI/B-27
SMCs, medium with PDGF-BB+TGF-β1
ECs, medium with VEGF+bFGF+BMP4
H
NC
2C
CMs
SMCs
ECs
TNNT2
SMA
TNNT2/SMA/DAPI
DAPI
SMA/DAPI
CD31
CD144
CD31/CD144/DAPI
100 μm

465 **Figure 3. Lineage tracing demonstrated 2C induced dedifferentiation of TNNT2$^+$ CMs to ISL1-**
466 **expressing RCCs. (A)** Immunofluorescence images showing expression of endogenous ISL1 (green) and
467 ISL1-mCherry (red) reporter in the cells differentiated from K9 hESC KI reporter line at day 6 (D6). DAPI
468 (4′,6-diamidino-2-phenylindole) staining labeled nuclei as blue. **(B-C)** Flow cytometry analysis of the
469 percentage of mCherry$^+$/ISL1$^+$ cells in the cells differentiated from K9 at D6. **(D-E)** Flow cytometry analysis
470 of the percentage of mCherry-negative cells at selection day 4 (SD4) in lactate purification medium. **(F)**
471 Cells induced from mCherry-negative CMs by treatment with or without 2C for 60 hours. Images showing
472 the expression of mCHERRY (red) and TNNT2 (green) in the cells. **(G)** Relative gene expression of *ISL1*,
473 *mCHERRY*, *LEF1*, *TNNT2* and *MYL2* in K9-derived mCherry-negative CMs treated with DMSO (NC) or 2C
474 for 60 hours. Data are shown as mean ± SD (n=2 independent experiments with 4 replicates each). Two-
475 way ANOVA with Šidák's multiple comparisons test. ***P < 0.001, ****P < 0.0001. **(H-I)** Flow cytometry
476 analysis of the percentage of mCherry-positive cells induced from mCherry-negative CMs by treatment with
477 or without 2C for 60 hours. Data are shown as mean ± SD (n=3 independent experiments, represented as
478 dots). **(J-K)** Flow cytometric plots showing EGFP-labeled CMs by lineage-tracing of K9-derived mCherry-
479 negative CMs (**J**), and bar graph showing the percentage of mCherry-negative CMs expressing EGFP (**K**).
480 Data are shown as mean ± SD (n=3 independent experiments). **(L)** Images showing the expression of ISL1
481 (red) and EGFP (green) in the cells induced from EGFP-positive/mCherry-negative CMs by treatment with
482 or without 2C for 60 hours. DAPI (4′,6-diamidino-2-phenylindole) staining labeled nuclei as blue.

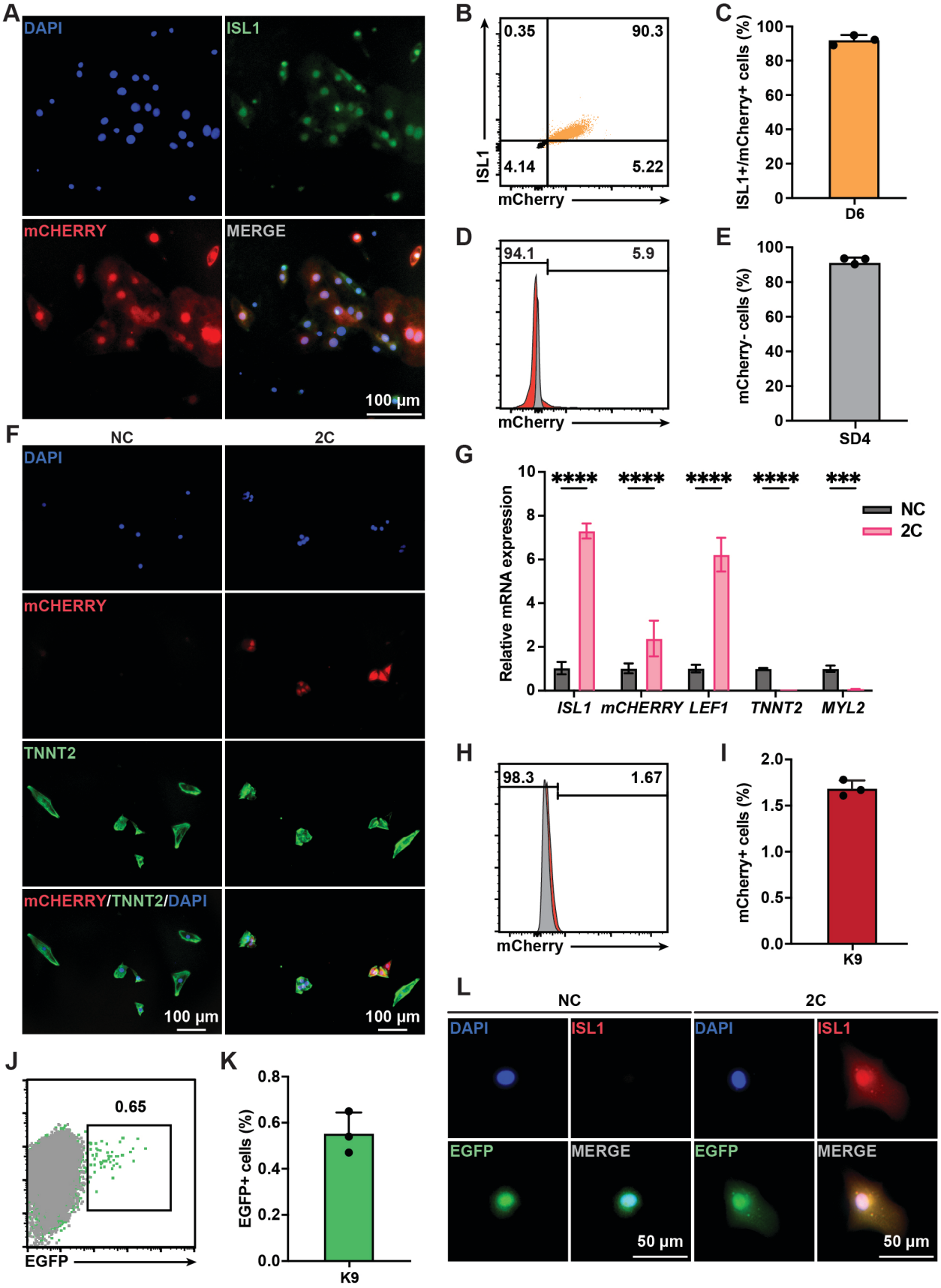
A
DAPI
ISL1
mCHERRY
MERGE
100 μm
B
0.35
90.3
4.14
5.22
ISL1
mCherry
C
ISL1+/mCherry+ cells (%)
100
80
60
40
20
0
D6
D
94.1
5.9
mCherry
E
mCherry- cells (%)
100
80
60
40
20
0
SD4
F
NC
2C
DAPI
mCHERRY
TNNT2
mCHERRY/TNNT2/DAPI
100 μm
100 μm
G
Relative mRNA expression
10
8
6
4
2
0
****
****
****
****
***
NC
2C
ISL1
mCHERRY
LEF1
TNNT2
MYL2
H
98.3
1.67
mCherry
I
mCherry+ cells (%)
2.0
1.5
1.0
0.5
0.0
K9
J
0.65
EGFP
K
EGFP+ cells (%)
0.8
0.6
0.4
0.2
0.0
K9
L
NC
2C
DAPI
ISL1
DAPI
ISL1
EGFP
MERGE
EGFP
MERGE
50 μm
50 μm

483

484 **Figure 4. Heart regeneration *via* 2C-induced dedifferentiation of CMs. (A)** Immunofluorescence
485 staining of ISL1 (green) and TNNT2 (red) in cross-sectioned hearts from 2C or vehicle (DMSO)-treated
486 (NC) adult 129SvJ mice. Ao, aorta. PA, pulmonary artery. LA, left atrial. RA, right atrial. IAS, interatrial
487 septum. DAPI (4′,6-diamidino-2-phenylindole) staining labeled nuclei as blue. **(B)** Schematic illustration of
488 the method used to examine the prophylactic effect of 2C in 129SvJ mice post MI. **(C)** Body weight of mice
489 pre-treated with vehicle (DMSO) or 2C as shown in (**B**) at Day 12, Day 16, Day 20, and Day 35 after MI
490 (dpi). Error bars represent SD. ns, not significant ($P > 0.05$). **(D)** Survival curve of sham-operated mice and
491 mice pre-treated with vehicle (DMSO) or 2C as shown in (**B**), at indicated time points before or after MI. **(E)**
492 Ejection fraction (EF) of sham-operated mice and mice pre-treated with vehicle (DMSO) or 2C as shown in
493 (**B**), before MI (baseline) or at Day 1, Day 8, Day 25, and Day 35 after MI (dpi). Data are shown as mean ±
494 SD. Two-way ANOVA with Tukey's multiple comparisons test. ns, not significant ($P > 0.05$), **$P < 0.01$, ***$P$
495 $< 0.001$. **(F)** Schematic illustration of the method used to examine therapeutic effect of 2C in the 129SvJ
496 mice post MI. **(G)** Serial fMRI measurements showing the cardiac function from sham-operated mice and
497 mice treated with vehicle (DMSO) or 2C at as shown in (**F**). Data are shown as mean ± SD. Two-way
498 ANOVA with Tukey's multiple comparisons test. *$P < 0.05$. **(H)** Echocardiography of sham-operated mice
499 and mice treated with vehicle (DMSO) or 2C as shown in (**F**) at Day 35 post MI. **(I)** Masson staining of serial
500 transverse sections of hearts from sham-operated mice and mice treated with vehicle (DMSO) or 2C as
501 shown in (**F**) at Day 35 post MI.

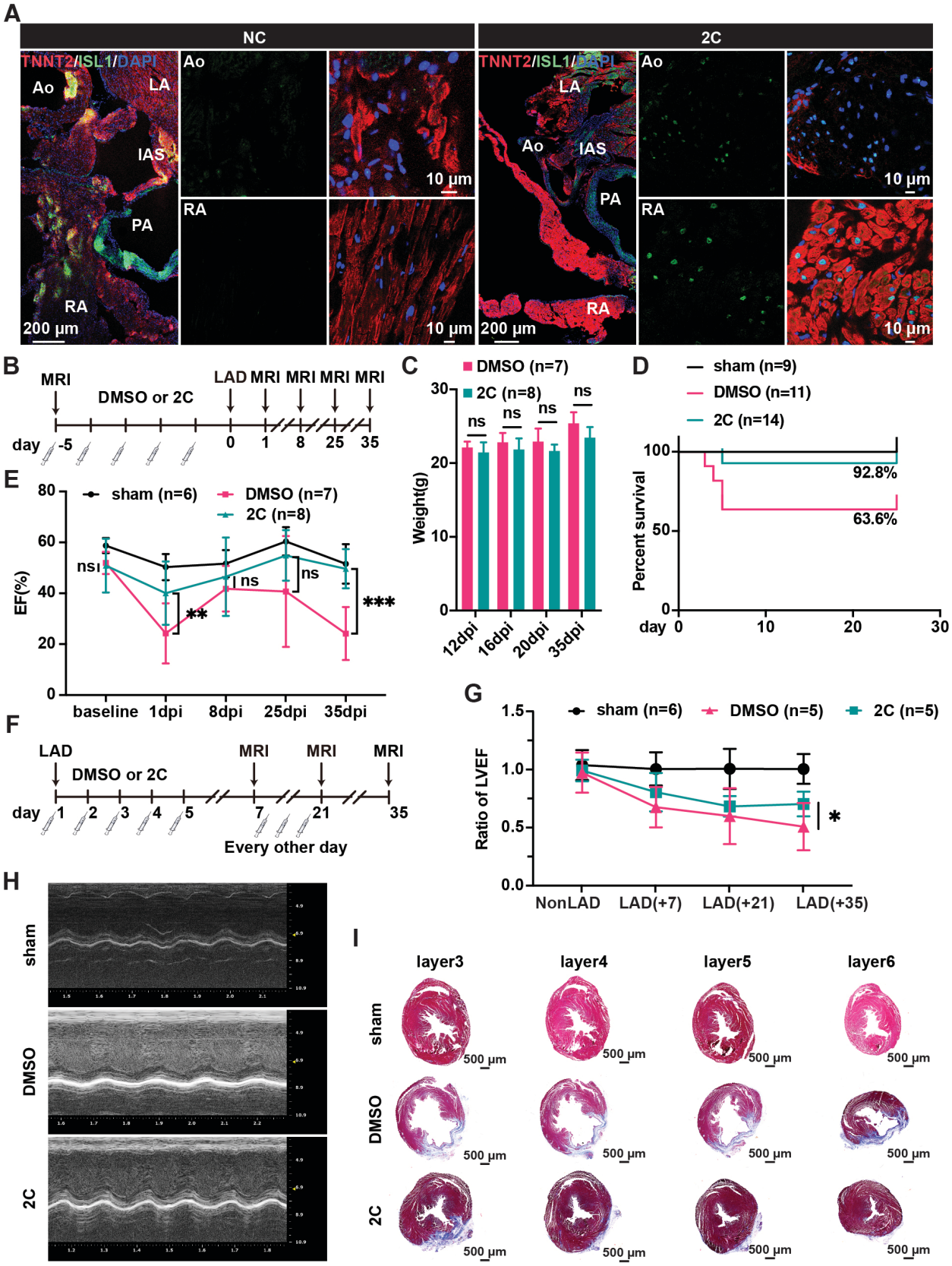
A
NC
2C
TNNT2/ISL1/DAPI
Ao
LA
IAS
PA
RA
200 μm
10 μm
B
MRI
DMSO or 2C
LAD MRI MRI MRI MRI
day -5 0 1 8 25 35
C
DMSO (n=7)
2C (n=8)
Weight(g)
ns
12dpi 16dpi 20dpi 35dpi
D
sham (n=9)
DMSO (n=11)
2C (n=14)
Percent survival
92.8%
63.6%
day 0 10 20 30
E
sham (n=6)
DMSO (n=7)
2C (n=8)
EF(%)
ns
**
***
baseline 1dpi 8dpi 25dpi 35dpi
F
LAD
DMSO or 2C
MRI MRI MRI
day 1 2 3 4 5 7 21 35
Every other day
G
sham (n=6)
DMSO (n=5)
2C (n=5)
Ratio of LVEF
*
NonLAD LAD(+7) LAD(+21) LAD(+35)
H
sham
DMSO
2C
I
layer3
layer4
layer5
layer6
500 μm

502

503 **Figure 5. Bulk RNA-seq of analysis of 2C-treated ISL1/mCherry-negative CMs. (A)** Scheme of bulk
504 RNA-seq analysis of K9-derived mCherry-negative CMs with DMSO (NC) or 2C treatment for 60 hours. **(B)**
505 Heatmap of differentially expressed genes (DEGs) in ISL1/mCherry-negative CMs treated with DMSO (NC)
506 or 2C for 60 hours. **(C)** Volcano plot showing genes significantly changed by 60 hours of 2C treatment. **(D-**
507 **E)** Gene Ontology (GO) analysis of downregulated (**D**) and upregulated (**E**) genes in ISL1/mCherry-
508 negative CMs by 2C treatment for 60 hours, compared to DMSO (NC) treated cells. **(F)** Plotting GO terms
509 of upregulated genes by 2C treatment with cnetlpot. **(G)** Relative expression fold-changes of indicated
510 genes in K9-derived ISL1/mCherry-negative CMs by 60 hours of DMSO (NC) or 2C treatment. Data are
511 shown as mean ± SD. Multiple unpaired t tests. **P < 0.01, ***P < 0.001.

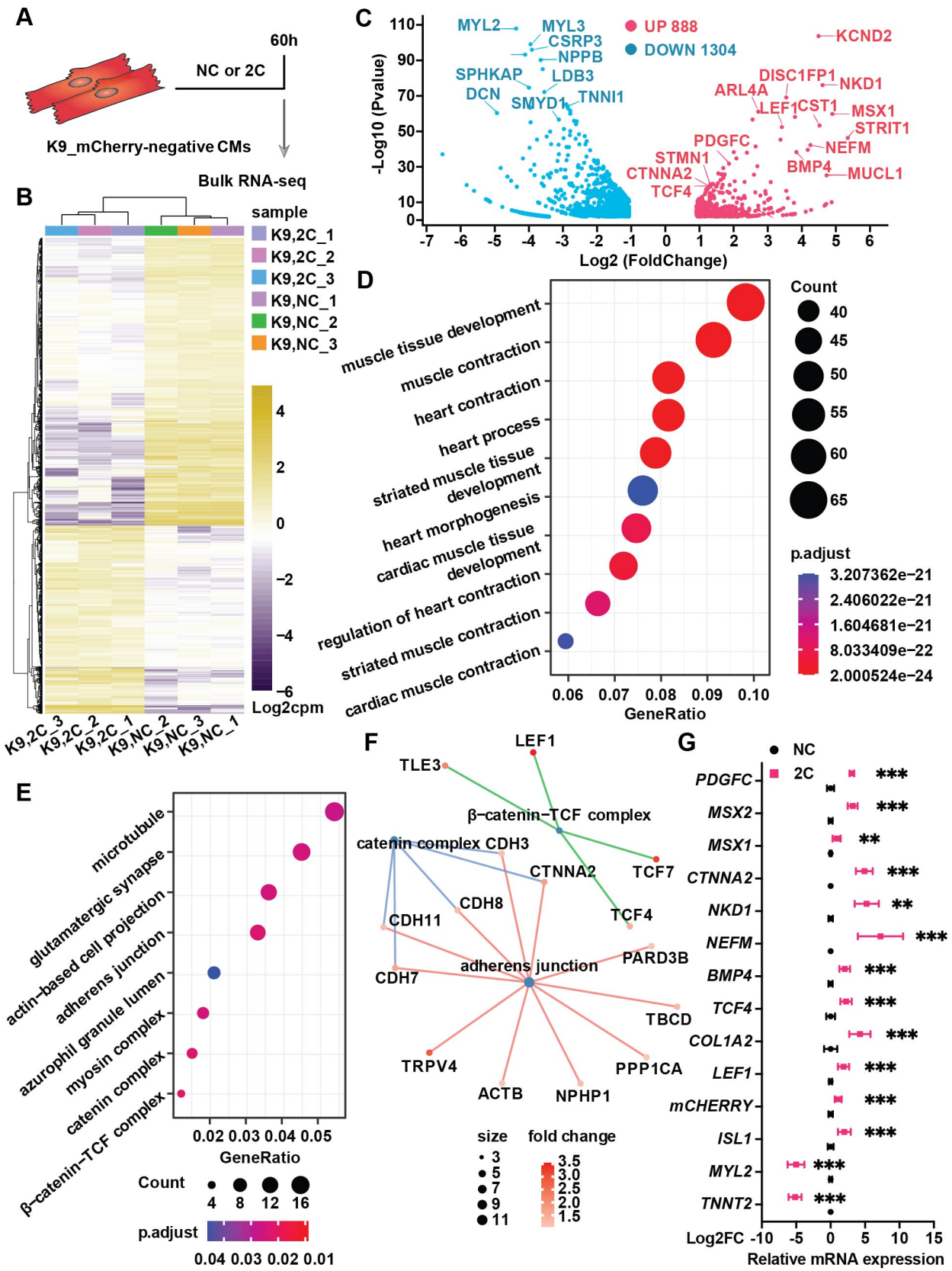
A
60h
NC or 2C
K9_mCherry-negative CMs
Bulk RNA-seq
B
sample
K9,2C_1
K9,2C_2
K9,2C_3
K9,NC_1
K9,NC_2
K9,NC_3
Log2cpm
C
UP 888
DOWN 1304
-Log10 (Pvalue)
Log2 (FoldChange)
MYL2
MYL3
CSRP3
NPPB
SPHKAP
LDB3
DCN
SMYD1
TNNI1
KCND2
DISC1FP1
NKD1
ARL4A
LEF1
CST1
MSX1
STRIT1
PDGFC
NEFM
STMN1
BMP4
CTNNA2
MUCL1
TCF4
D
muscle tissue development
muscle contraction
heart contraction
heart process
striated muscle tissue development
heart morphogenesis
cardiac muscle tissue development
regulation of heart contraction
striated muscle contraction
cardiac muscle contraction
GeneRatio
Count
p.adjust
E
microtubule
glutamatergic synapse
actin-based cell projection
adherens junction
azurophil granule lumen
myosin complex
catenin complex
β-catenin-TCF complex
GeneRatio
Count
p.adjust
F
LEF1
TLE3
β-catenin-TCF complex
catenin complex CDH3
CTNNA2
TCF7
CDH8
TCF4
CDH11
adherens junction
PARD3B
CDH7
TBCD
TRPV4
PPP1CA
ACTB
NPHP1
size
fold change
G
NC
2C
PDGFC
MSX2
MSX1
CTNNA2
NKD1
NEFM
BMP4
TCF4
COL1A2
LEF1
mCHERRY
ISL1
MYL2
TNNT2
Log2FC
Relative mRNA expression

512

513 **Figure 6. Single-cell RNA-seq of 2C-treated mCherry-negative CMs. (A)** UMAP analysis showing 7
514 clusters in cells induced from K9-derived mCherry-negative CMs by treatment with DMSO (NC) and 2C for
515 60 hours. **(B)** The percentage of cells in the 7 indicated clusters, following DMSO (NC) or 2C treatment. **(C)**
516 Heatmap showing the differentially expressed genes in the cells from 7 indicated clusters. The
517 representative marker genes of 7 indicated clusters were listed on the right. **(D)** Violin plots showing the
518 expression levels of marker genes of CMs (MYL2, MYH6), ICs (COL1A1, ACTA2), and RCCs (ISL1, BMP4,
519 FGF20) among cells from 7 indicated clusters. **(E)** UMAP analysis showing the second-level clustering of
520 cluster 2 into 4 subclusters (left), which exhibited dramatic distinction under condition of 2C or NC (right).
521 **(F)** The percentage of cells in the 4 indicated subclusters within cluster 2, following DMSO (NC) or 2C
522 treatment. **(G)** Heatmap showing the differentially expressed genes among cells from 4 subclusters of
523 cluster 2. Genes related to RCCs are highlighted in the green blocks on the right. **(H-I)** Pseudotime trajectory
524 showing changes across various cell states upon 2C treatment, which were presented with different
525 developmental pseudotime points (**H**) and cell states (**I**). **(J)** Curves showing the dynamic expression of
526 representative genes of RCCs (ISL1, FGF20), ICs (COL1A1), and CMs (TNNT2) along indicated
527 pseudotime points.

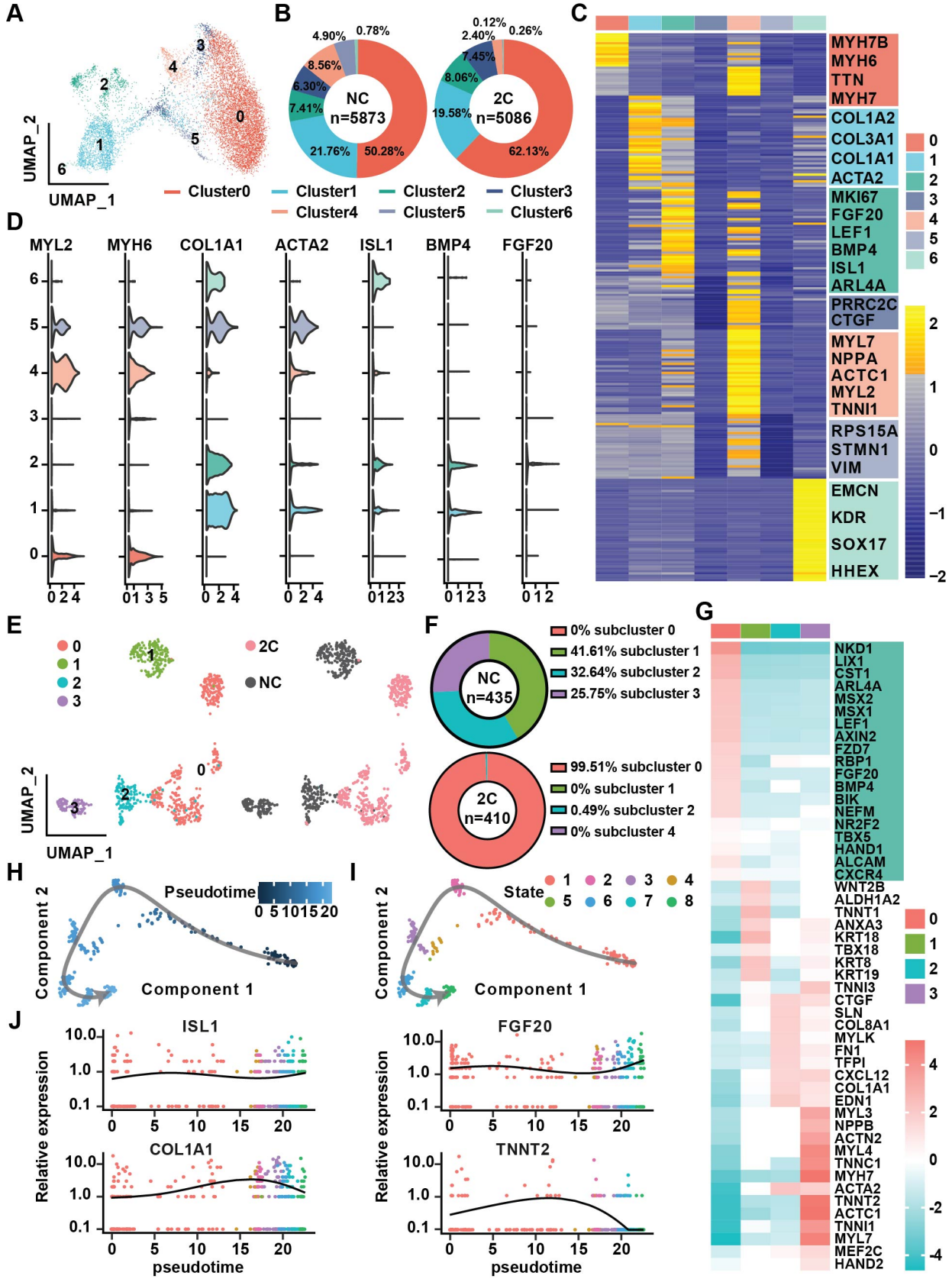
A
UMAP_2
UMAP_1
Cluster0
Cluster1
Cluster2
Cluster3
Cluster4
Cluster5
Cluster6
B
NC
n=5873
2C
n=5086
C
MYH7B
MYH6
TTN
MYH7
COL1A2
COL3A1
COL1A1
ACTA2
MKI67
FGF20
LEF1
BMP4
ISL1
ARL4A
PRRC2C
CTGF
MYL7
NPPA
ACTC1
MYL2
TNNI1
RPS15A
STMN1
VIM
EMCN
KDR
SOX17
HHEX
D
MYL2
MYH6
COL1A1
ACTA2
ISL1
BMP4
FGF20
E
2C
NC
F
NC
n=435
0% subcluster 0
41.61% subcluster 1
32.64% subcluster 2
25.75% subcluster 3
2C
n=410
99.51% subcluster 0
0% subcluster 1
0.49% subcluster 2
0% subcluster 4
G
NKD1
LIX1
CST1
ARL4A
MSX2
MSX1
LEF1
AXIN2
FZD7
RBP1
FGF20
BMP4
BIK
NEFM
NR2F2
TBX5
HAND1
ALCAM
CXCR4
WNT2B
ALDH1A2
TNNT1
ANXA3
KRT18
TBX18
KRT8
KRT19
TNNI3
CTGF
SLN
COL8A1
MYLK
FN1
TFPI
CXCL12
COL1A1
EDN1
MYL3
NPPB
ACTN2
MYL4
TNNC1
MYH7
ACTA2
TNNT2
ACTC1
TNNI1
MYL7
MEF2C
HAND2
H
Pseudotime
Component 2
Component 1
I
State
J
ISL1
COL1A1
FGF20
TNNT2
Relative expression
pseudotime

528

529 **Figure 7. Chromatin immunoprecipitation-sequencing (ChIP-seq) analyses of chemical-treated H9**
530 **hESC-derived CMs. (A)** Schematic illustration of ChIP-seq analysis of H9-derived CMs subjected to DMSO,
531 A-485, CHIR99021, or 2C treatment for 60 hours. **(B)** Average ChIP-seq signal profiles showing the
532 indicated histone modifications around the TSS in the input and ChIP samples prepared from DMSO and
533 2C-treated cells. **(C)** Heatmap showing the whole-genome wide distribution of H3K9Ac, H3K27Ac, and
534 H3K4me3 peaks within a range of ±4kb from TSSs in the cells treated with DMSO or 2C for 60 hours. **(D)**
535 H3K9Ac and H3K27Ac peaks surrounding CM genes (TNNT2 and TNNI1) and RCC genes (LEF1 and ISL1)
536 in the cells treated with DMSO, A-485, CHIR99021 or 2C for 60 hours, and H3K4me3 peaks surrounding
537 the same genes in the cells treated by DMSO or 2C. The y-axis represents the number of counts. **(E-F)**
538 Veen diagram showing the number of annotated genes with H3K9Ac or H3K27Ac enrichment in the cells
539 treated with DMSO, A-485, CHIR99021 or 2C for 60 hours. Red circles indicate the number of genes with
540 unique H3K9Ac or H3K27Ac enrichment induced by 2C treatment; black circles indicate the number of
541 genes with H3K9Ac or H3K27Ac enrichment unaffected by any chemical treatment. **(G-J)** The annotated
542 genes with the most significant changes in H3K9Ac enrichment following treatment with DMSO (**G**) or 2C
543 (**I**) were ranked by Log10LR and analyzed by GOs (**H** and **J**), respectively. **(K)** ISL1 binding motifs identified
544 from the cells treated with A-485 or 2C.

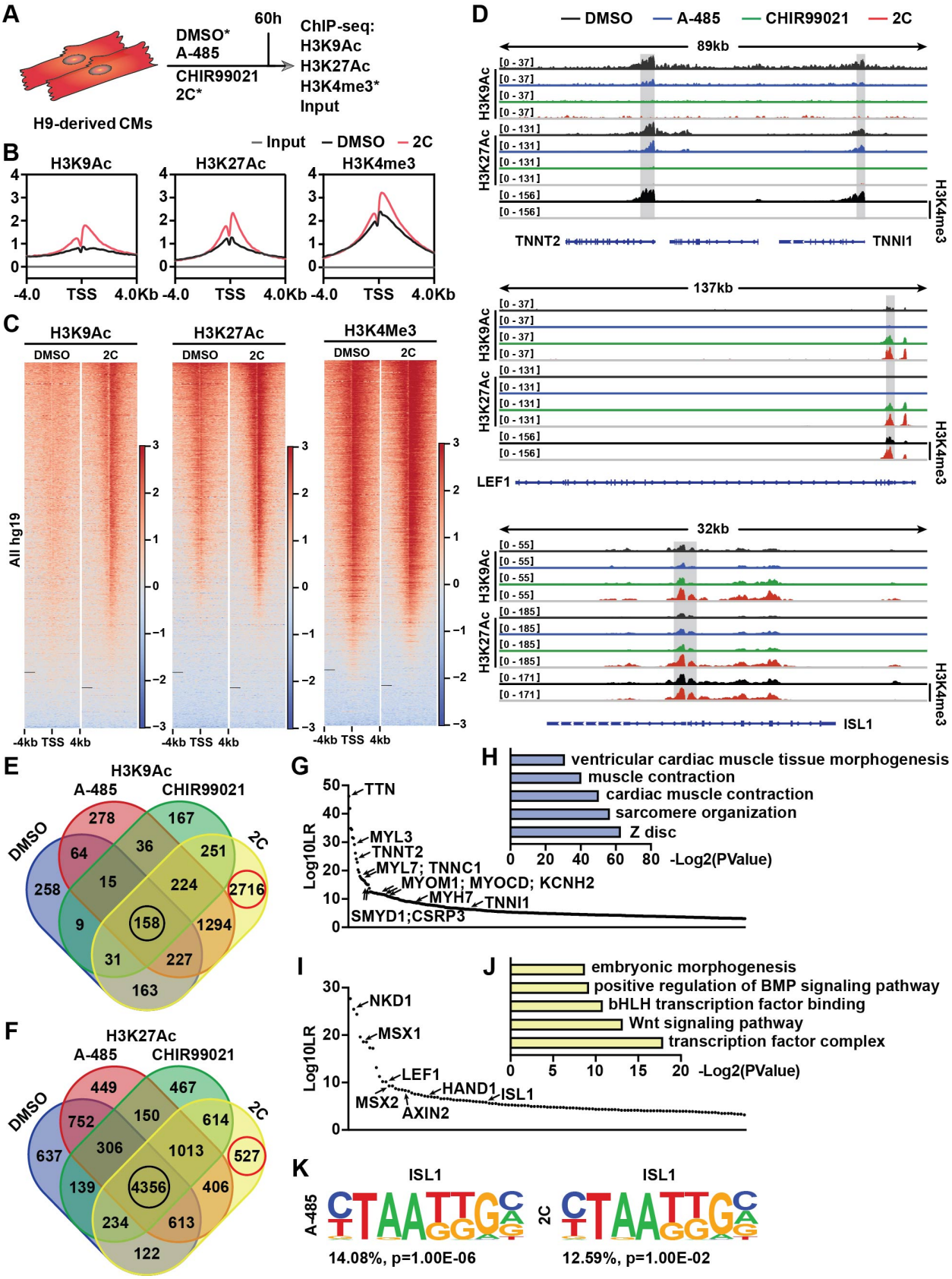
A
H9-derived CMs
DMSO*
A-485
CHIR99021
2C*
60h
ChIP-seq:
H3K9Ac
H3K27Ac
H3K4me3*
Input
B
Input
DMSO
2C
H3K9Ac
H3K27Ac
H3K4me3
-4.0
TSS
4.0Kb
C
H3K9Ac
H3K27Ac
H3K4Me3
DMSO
2C
All hg19
-4kb TSS 4kb
D
DMSO
A-485
CHIR99021
2C
89kb
H3K9Ac
H3K27Ac
H3K4me3
TNNT2
TNNI1
137kb
LEF1
32kb
ISL1
E
H3K9Ac
A-485
CHIR99021
DMSO
2C
278
167
64
36
251
258
15
224
2716
9
158
1294
31
227
163
F
H3K27Ac
A-485
CHIR99021
DMSO
2C
449
467
752
150
614
637
306
1013
527
139
4356
406
234
613
122
G
Log10LR
TTN
MYL3
TNNT2
MYL7; TNNC1
MYOM1; MYOCD; KCNH2
MYH7
TNNI1
SMYD1;CSRP3
H
ventricular cardiac muscle tissue morphogenesis
muscle contraction
cardiac muscle contraction
sarcomere organization
Z disc
-Log2(PValue)
I
Log10LR
NKD1
MSX1
LEF1
HAND1
ISL1
MSX2
AXIN2
J
embryonic morphogenesis
positive regulation of BMP signaling pathway
bHLH transcription factor binding
Wnt signaling pathway
transcription factor complex
-Log2(PValue)
K
A-485
ISL1
14.08%, p=1.00E-06
2C
ISL1
12.59%, p=1.00E-02

545